Electron paramagnetic resonance study of Fe^{3+} in α-quartz: Hydrogen-compensated center

M. J. Mombourquette
Department of Physics, Oklahoma State University, Stillwater, Oklahoma 74078
and Department of Chemistry, University of Saskatchewan, Saskatoon, Saskatchewan, Canada S7N 0W0

J. Minge*
Department of Chemistry, University of Saskatchewan, Saskatoon, Saskatchewan, Canada S7N 0W0

M. R. Hantehzadeh
Department of Physics, Oklahoma State University, Stillwater, Oklahoma 74078

J. A. Weil
Department of Chemistry, University of Saskatchewan, Saskatoon, Saskatchewan, Canada S7N 0W0

L. E. Halliburton
Department of Physics, Oklahoma State University, Stillwater, Oklahoma 74078
(Received 6 September 1988)

Electron paramagnetic resonance and proton electron-nuclear double-resonance studies of a hydrogen-compensated Fe^{3+} ($S=\frac{5}{2}$) center in synthetic iron-doped α-quartz have been carried out at 20 and 15 K, respectively. The spin-Hamiltonian parameters were determined, allowing anisotropy of the g matrix as well as [g, D, A (^{1}H)]-matrix noncoaxiality, and including high-spin terms of the form S^4. Evaluation of the results gives strong evidence that the center (called S_2 by some workers) consists of a Fe^{3+} ion occurring substitutionally at a Si^{4+} site, charge compensated by an interstitial hydrogen ion. The label $[FeO_4/H^+]^0$ is proposed for the center.

I. INTRODUCTION

We are continuing detailed electron paramagnetic resonance (EPR) and electron-nuclear double-resonance (ENDOR) studies of naturally occurring and radiation-induced paramagnetic centers in α-quartz. The present work includes the results of experiments on hydrogen-diffused synthetic iron-doped crystals. The strongest lines occurring as a result of the diffusion process are ascribed to the hydrogen-compensated iron center sometimes called S_2 by earlier workers.[1-4] To date, there are no experimental studies which give quantitative EPR parameters of this center or conclusively explain its structure.

In an earlier work[5] we reported EPR results on the center we call $[FeO_4]^-$ (denoted in other works by S_0 or I) and provided evidence that the Fe^{3+} ion (in this case) substitutes for a Si^{4+} in quartz with no local charge compensation. The $[FeO_4]^-$ center exhibits twofold symmetry and relatively little distortion from the silicon-site surroundings. The hydrogen-compensated center described in the present paper does not exhibit such twofold symmetry, consistent with the proton bonding directly to one of the oxygens in the pseudotetrahedron provided by the nearest-neighbor oxygen ions around the iron. We are interested in comparing the two centers as part of a general study of four iron centers in quartz, $[FeO_4]^-$, $[FeO_4/Li^+]^0$, $[FeO_4/H^+]^0$, and $[FeO_4/Na^+]^0$ (denoted elsewhere by S_0, S_1, S_2, and S_3, respectively).

II. EXPERIMENT

The iron-doped crystalline cultured quartz used in this investigation was grown by Sawyer Research Products (Lakeland, Ohio) and was electrodiffused with protons at Oklahoma State University. The diffusion was carried out at $\sim 500\,^\circ$C in a H_2 atmosphere with an applied electric field of ~ 2000 V/cm (voltage across the plate on which gold electrodes had been deposited). The yellow-brown crystal was oriented initially using morphology and several EPR samples were cut, each with dimensions $\sim 10\times 2\times 1.5$ mm^3 such that the longest dimension was approximately parallel to one ($\equiv \hat{\mathbf{a}}_1$) of the three twofold axes in the quartz crystal and the smallest dimension was along **c** (the threefold screw axis).

Before the hydrogen electrodiffusion, the samples displayed intense signals from the center $[FeO_4/Li]^0$. Afterwards, there was still considerable signal from $[FeO_4/Li]^0$ and also a strong signal which we have now identified as $[FeO_4/H]^0$. One of the diffused samples was irradiated with x rays for 1 h at room temperature. The irradiated crystal displayed amethyst coloration and also showed a significant increase in the EPR signal intensity of the hydrogen-compensated center and a greatly re-

duced signal from the lithium-compensated center. The irradiated (and diffused) crystal was then mounted in the EPR cavity with $\hat{\mathbf{a}}_1$ vertical. The crystal was accurately oriented (± 1 min of arc) by adjusting to achieve superposition of appropriate symmetry-related EPR lines for all orientations of $\hat{\mathbf{B}}$ in the horizontal plane, i.e., three doubly degenerate species of lines observed for each type of transition.[6] To describe a general orientation of the external magnetic field vector $\hat{\mathbf{B}}$ relative to the crystallographic axes $\hat{\mathbf{c}}$, and $\hat{\mathbf{a}}_i$ ($i=1,2,3$), polar angle θ and azimuthal angle ϕ are used, where $\theta=\angle(\hat{\mathbf{c}},\hat{\mathbf{B}})$ and $\phi=\angle(\hat{\mathbf{a}}_1$, the projection of $\hat{\mathbf{B}}$ onto plane $\perp\hat{\mathbf{c}})$. An EPR data set was collected at 20 K using a low-temperature EPR cavity system[7] and a Varian V4502 spectrometer operated at a frequency of ~ 9.93 GHz. Our frequency and field data had estimated uncertainties of 1×10^{-6} GHz and 1×10^{-3} mT, respectively. The magnetic field was calibrated using a proton NMR gaussmeter, and at ~ 320 mT using the well-characterized[8] center $[AlO_4]^0$ which was also present in our irradiated sample. A constant correction was added to all measured magnetic fields to take into account, in first approximation, the difference in position between the NMR probe and the quartz sample. Rotation data were collected in 10° steps (1° near turning points) at angles measured with a precision of ± 2 min of arc, over a 180° range in the plane $\hat{\mathbf{B}}\perp\hat{\mathbf{a}}_1$. All observable transitions (see Fig. 5) were explored, with special attention paid at the line-position turning points. Also present were extraneous weaker lines, arising from the $[FeO_4]^0$ center, the $[FeO_4/Li]^0$ center, and the three-hydrogen and four-hydrogen centers previously reported,[9] plus some still weaker as yet unidentified lines.

The EPR lines for the $[FeO_4/H]^0$ center were clearly visible from 20 K to room temperature and showed no qualitative changes with temperature in that range. No data set has yet been collected at room temperature so that no quantitative discussion of thermal effects is possible.

The EPR linewidths are appreciably greater for center $[FeO_4/H]^0$ than for those (0.02 mT) of other noniron centers in quartz and depend somewhat on orientation. The lines tend to be broadest at orientations where the slope of the line position versus angle (about $\hat{\mathbf{a}}_1$) is steepest. Typically, the full width between extrema of the first derivative is ~ 0.3 mT.

At most orientations, the $[FeO_4/H]^0$ spectra contain satellites from ^{57}Fe and possibly from ^{29}Si. The ^{57}Fe lines were identified by measuring the intensity of the hyperfine lines compared to that of the main lines: the measured ratio of intensities agrees with the ratio of abundances between ^{57}Fe (2.15%) and the even isotopes (^{56}Fe, etc). The spacing was close to isotropic with a value of ~ 1 mT.

At most orientations, hyperfine splittings from a single hydrogen nucleus were visible. In general, the number and pattern of hyperfine lines observed was consistent with the number of lines expected when the nuclear magnetic moment interacts appreciably both with the electronic spin moment and with the externally applied magnetic field (termed the direct field effect).[10] In this situation, a maximum of $2S(2I+1)^2$ lines is visible. For our case, $S=\frac{5}{2}$ and $I=\frac{1}{2}$, we expect (and find) 20 primary lines per site, i.e., each of five electronic transitions is split into four via the hyperfine interaction (see Fig. 1). The actual single-proton hyperfine structure on each transition manifests itself as either a doublet, triplet (see Fig. 2), or quartet, depending on the location and relative intensities of the normally forbidden ($\Delta m_I \neq 0$) transitions.

Electron-nuclear double-resonance measurements were made using a Bruker ER200 EPR spectrometer with a Bruker Model 250 ENDOR accessory. The data-acquisition system used is an Aspect 2000 computer interfaced with the EPR spectrometer. The ENDOR cavity resonated in the TM_{011} mode. The rf magnetic field at the sample was created using a rf helix mounted on a quartz variable temperature Dewar inserted in the microwave cavity, allowing for a wide range of operating frequencies ranging from 0.5 to 100 MHz with modulation depths up to 500 kHz. The ENDOR sample was cooled to 15 K by an Oxford EPR-900 continuous-flow system. Precise alignment of the crystal, as was done for the EPR measurements, was not possible in taking the ENDOR measurements (due to space restrictions in the ENDOR cavity). To overcome this problem, both EPR and ENDOR measurements were made on the crystal at each orientation of the crystal while mounted in the ENDOR cavity. The spin-Hamiltonian parameters, derived

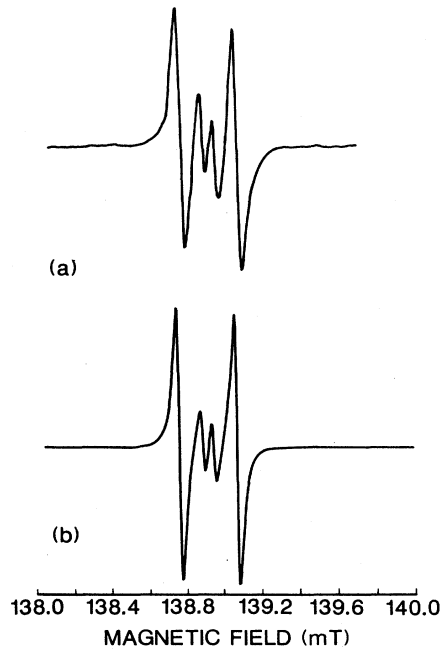

FIG. 1. First-derivative EPR spectrum at 9.915 GHz, showing the ^1H hyperfine lines of the $3\leftrightarrow4$ (high-field quantum numbers m_s: $-\frac{1}{2}\leftrightarrow\frac{1}{2}$) transition (site 1) at crystal orientation $\theta=20°$, $\varphi=90°$ (where θ is the polar angle measured from $\hat{\mathbf{c}}$ and φ is the azimuthal angle measured from $\hat{\mathbf{a}}_1$). (a) Experimental spectrum taken at ~ 20 K. Note the weak ^{57}Fe lines at the wings. (b) Spectrum simulated from the spin-Hamiltonian parameters of Table I.

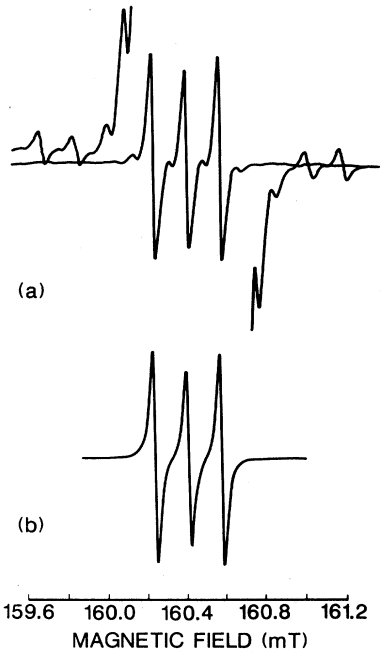

FIG. 2. First-derivative EPR spectrum at 9.915 GHz, showing the ^{1}H hyperfine lines of the 3↔4 (m_s: $-\frac{1}{2}\leftrightarrow\frac{1}{2}$) transition (site 1) at crystal orientation $\theta=0°$. (a) Experimental spectrum taken at ~20 K. Note the weak ^{57}Fe hydrogen triplets as well as additional lines at the wings arising presumably from ^{29}Si (4.67%). (b) Spectrum simulated from the spin-Hamiltonian parameters of Table I.

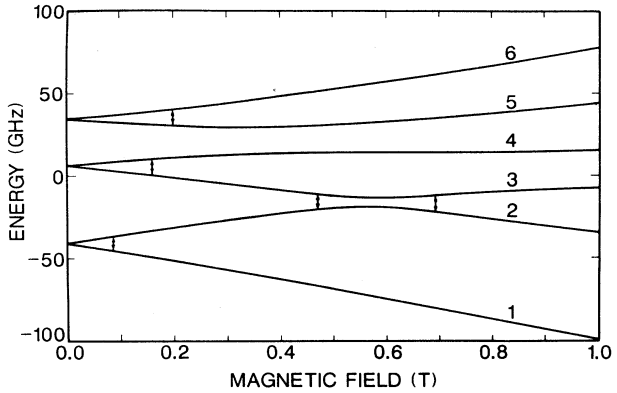

FIG. 3. The energy levels for $[FeO_4/H]^0$ as a function of external magnetic field ($\hat{\mathbf{B}}\|\hat{\mathbf{c}}$). No hyperfine splittings are included. Transitions at 9.915 GHz are indicated, and occur at (calculated) fields 96.47, 160.45, 198.76, 465.56, and 686.40 mT. The levels corresponding to the high-field m_s quantum numbers $-\frac{5}{2}$, $-\frac{3}{2}$, $-\frac{1}{2}$, $\frac{1}{2}$, $\frac{3}{2}$, and $\frac{5}{2}$ are numbered in order (increasing energy) from 1 to 6.

from the EPR data measured on the well-aligned crystal, were then used along with EPR lines measured on the poorly aligned crystal in the ENDOR cavity to determine the crystal's actual alignment during the ENDOR measurements. The hydrogen hyperfine matrix was then fitted using the ENDOR data with the calculated crystal orientations.

The spin Hamiltonian used for $[FeO_4/H]^0$ is similar to the one described by Mombourquette *et al.*[5] for $[FeO_4]^-$, except that in our present case there is no twofold symmetry and thus simplification of the parameter set using symmetry constraints described therein is not valid. In addition, a hyperfine term of form $\mathbf{S}\cdot\mathbf{A}\cdot\mathbf{I}$ plus an isotropic nuclear Zeeman term $-g_H\beta_n\mathbf{I}\cdot\mathbf{B}$ was required for the ^{1}H nuclear effects.

To identify among the six sites the two symmetry-related sites (1 and 1′) which have their Fe^{3+} ions located on (or near) crystal twofold axis $\hat{\mathbf{a}}_1$, it proved convenient to compare the six sets of symmetry-related spin-Hamiltonian parameters with those of center $[FeO_4/Na]^0$, for which the identification could be made from thermal studies.[11] For corroboration, a crystal of Brazilian natural amethyst having an uneven distribution

TABLE I. Center $[FeO_4/H]^0$ principal values and directions of matrices $Y=g$, D, and A (^{1}H) in the crystal Cartesian coordinate system [Ref. 5, Table II: coordinate system (1)] for site 1 at ~20 K, derived from EPR data. The S^4 parameters B_4^m are included as well (Ref. 5). The estimated uncertainties are included, in parentheses.

		Y		k	Y_k	θ_k	φ_k
g	2.004 45(19)	−0.000 33(11)	0.000 64(8)	1	2.004 02(15)	115.7(3.5)	17.6(8.5)
		2.004 94(15)	−0.000 08(8)	2	2.004 94(14)	65.7(5.2)	95.1(7.6)
			2.005 23(12)	3	2.005 67(12)	36.7(3.4)	327.8(6.4)
D/h (MHz)	−951.2(9)	2643.0(4)	−4166.5(6)	1	5807.7(6)	68.977(5)	81.389(8)
		3847.2(5)	4014.0(5)	2	2312.2(5)	55.003(3)	186.998(11)
			−2896.0(8)	3	−8119.9(5)	42.569(3)	326.656(4)
$A(^1H)/h$ (MHz)	6.5(8)	−0.4(6)	5.2(6)	1	−4.6(3)	72(24)	96(15)
		−4.5(4)	−0.5(4)	2	−3.9(9)	147(15)	36(43)
			−1.4(7)	3	9.1(6)	64(2)	357(3)
B_4^m/h (MHz)	B_4^0/h 0.44(2)						
	B_4^1/h 0.10(7)		B_4^2/h −1.66(6)		B_4^3/h −2.43(15)		B_4^4/h 3.95(6)
	B_4^{-1}/h 3.17(9)		B_4^{-2}/h 2.22(6)		B_4^{-3}/h 4.08(19)		B_4^{-4}/h 1.43(5)

TABLE II. Center $[FeO_4/H]^0$ principal values and directions of matrix $Y = A(^1H)$ in the crystal Cartesian coordinate system [Ref. 5, Table II: coordinate system (1)] for site 1 at ~15 K, derived from ENDOR data. The estimated uncertainties are included, in parentheses.

		Y		k	Y_k	θ_k	φ_k
$A(^1H)/h$ (MHz)	7.1(2)	0.2(4)	4.9(2)	1	−5.1(2)	65(13)	102(8)
		−4.7(1)	−0.6(6)	2	−3.5(4)	144(11)	52(17)
			−1.6(3)	3	9.3(2)	66(1)	360(2)

of iron ions among the sites was investigated. This crystal had a concentration of Fe^{3+} ions markedly lower on one of the crystallographic twofold axes $\hat{\mathbf{a}}_i$ than on the other two. The ions may in fact be slightly off axis, and we can indicate the resulting two sites by i and i'. With one axis ($\hat{\mathbf{a}}_1$) of the twofold axes aligned perpendicular to the magnetic field $\hat{\mathbf{B}}$, three EPR lines from a given transition were observed. These are doubly degenerate transitions arising from sites 1 and 1′, sites 2 and 3′, and sites 3 and 2′, respectively. Here 1, 2, and 3 are the indices i of the axes. An EPR spectrum was measured at an angle near c axis at which all the symmetry-related lines for a given EPR transition were resolved but relatively close together. If $\hat{\mathbf{a}}_1$ is the axis containing the lower Fe^{3+} concentration, then the line from sites 1 and 1′ will be the least intense of the three; otherwise, it will be the most intense. In either case, site 1 is uniquely identified.

III. RESULTS AND DISCUSSION

We have accurately determined the spin-Hamiltonian parameters including matrices g, D, and the $A(^1H)$ hyperfine matrix, as well as terms of order S^4. Terms of the type BS^3 and BS^5 were found to have no significant effect on the fitting results. The matrices g, D and the S^4 parameters were obtained from averaged EPR line positions (each taken as the center of gravity of the hydrogen hyperfine pattern). The final rms deviation between 195 calculated and observed EPR line positions was 0.08 mT. To find the $A(^1H)$ hyperfine matrix, a total of 390 individual line positions taken from 3-4 and 5-6 transitions (since ^1H hyperfine structure was clearly seen on low-field EPR lines only) was used. In the subsequent fitting procedure only $A(^1H)$ matrix elements were varied; the final rms deviation was 0.07 mT. The fit of 68 ENDOR frequencies (collected on the 3-4 EPR lines) gave final rms of 0.8 MHz (i.e., 0.03 mT). Results from the fitting are reported in Tables I (EPR) and II (ENDOR). Note that the hyperfine matrix derived from the EPR data and that from the ENDOR data are consistent to within experimental error and that the ENDOR data give slightly improved error limits for most of the fitted hyperfine parameters.

The signs of the S^2 parameters (D) and of the S^4 parameters are linked, i.e., the relative sign of any pair of such parameters is given by the fitting. Thus only the choice $\pm D$ is unavailable, except from very-low-temperature intensity measurements of the EPR lines. Such a determination was carried out by Matarrese

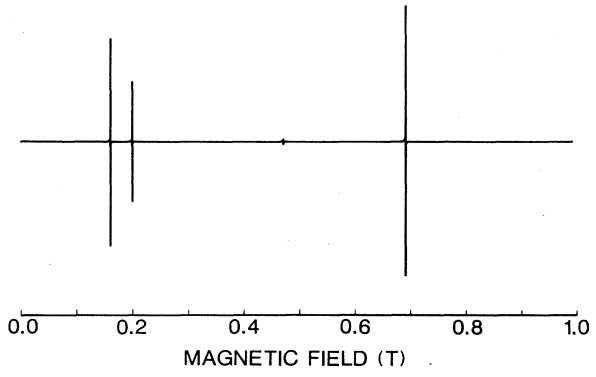

FIG. 4. EPR spectrum at 9.915 GHz simulated from the best-fit spin-Hamiltonian parameters in Table I, for $\hat{\mathbf{B}}\|\hat{\mathbf{c}}$ and excitation field $\hat{\mathbf{B}}_1\|\hat{\mathbf{a}}_1$. The transitions are also shown in Fig. 3. The ^1H hyperfine splitting (as in Fig. 1) is not visible at the field scale used. The spectrum agrees well with the observed one.

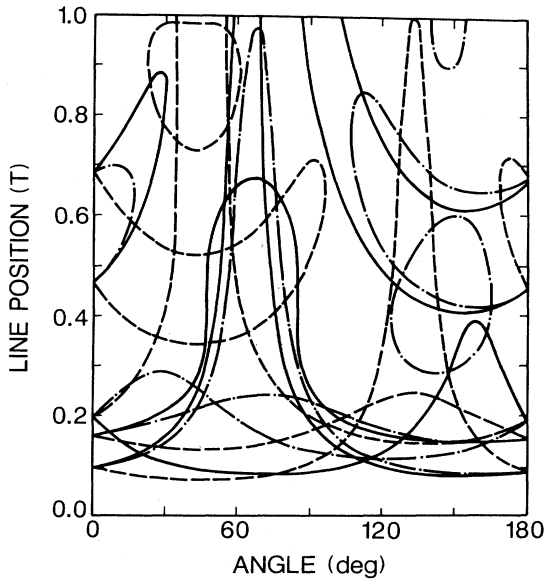

FIG. 5. EPR line positions at 9.915 GHz and $T = 20$ K as a function of crystal rotation about twofold axis $\hat{\mathbf{a}}_1$. The experimental data points are not shown explicitly, since on the vertical scale used, none would visibly deviate from the calculated curves shown. All symmetry-related sites are included, giving three doubly degenerate lines for each transition: solid curves, site 1 (and 1′); dashed curves, site 2 (and 2′); dashed-dotted curves, site 3 (and 3′). The ^1H hyperfine structure is not included. Angle 0° is at $\hat{\mathbf{B}}\|\hat{\mathbf{c}}$, and 90° is at $\hat{\mathbf{B}}\|\hat{\mathbf{y}}$ ($\perp\hat{\mathbf{a}}_1$ and $\hat{\mathbf{c}}$). The lines for all six symmetry-related $[FeO_4/H]^0$ sites superimpose at 0°.

et al.[12] for $[FeO_4]^-$; we have chosen the signs for $[FeO_4/H]^0$ consistent with this.

The sign choice $\pm A(^1H)$ is linked to the choice for D. In practice, equally good fits are obtained in both cases. However, the $A(^1H)$ matrix reported in Tables I and II was assigned the sign expected from theoretical considerations.

Figure 3 shows an energy-level diagram as a function of B, indicating the observed EPR transitions. A simulated c-axis spectrum is presented in Fig. 4. The line positions for crystal rotation about axis $\hat{\mathbf{a}}_1$ are detailed in Fig. 5.

In contrast to the situation with $[FeO_4]^-$,[5] the absence of symmetry about the crystal twofold axis suggests that the proton breaks the symmetry by bonding to an oxygen ion. Such effects occur in the $[TiO_4/H]^0$ center in α-quartz.[13]

We note that all three principal values of g are close to the free-electron value, as is to be expected for an S-state ion, and are close to those of g for the $[FeO_4]^-$ center.[5] The site-1 principal direction corresponding to the largest D value agrees nearly perfectly with one Si-$O_>$ direction in pure α-quartz ($\theta=43.5°$, $\phi=327.0°$; see Table V of Ref. 5), where $O_>$ stands for an oxygen atom with the longer type of bond to the central Si atom in the $[SiO_4]^0$ unit. We note also that the principal direction corresponding to the largest g value is close to the direction of the Si-$O_>$ bond.

The matrix $A(^1H)$ has a relatively small isotropic part (0.25 MHz) and is close to uniaxial (Tables I and II). The point-point dipolar model leads to a spin-spin distance of 2.6 Å. This appears to be a very reasonable value, especially in light of the calculated value of 2.44 Å obtained by Hartree-Fock calculation for $[AlO_4/H]^0$.[14] The Al-H direction given by $\theta=58.7°$ and $\phi=354.2°$ agrees nicely with the direction given in Tables I and II. These theoretical results are for H^+ bonded to a long-bonded oxygen ion; the proton on a short-bonded oxygen does not yield agreement with the data presented herein. A more detailed interpretation of the hyperfine matrix is difficult, especially without detailed knowledge of the spin-density distribution on the iron and oxygen ions. The insensitivity of the spin-Hamiltonian parameters to temperature suggests that the hydrogen bond is quite strong. Further experimental work is planned to attain such information. Comparison of the present results with similar data for centers $[FeO_4/Li]^0$ and $[FeO_4/Na]^0$, as well as $[FeO_4]^-$, will be presented in a subsequent publication.[11]

ACKNOWLEDGMENTS

The authors wish to thank A. S. Nowick and J. J. Martin for making the samples available. This work was supported in part by the Natural Sciences and Engineering Research Council of Canada and by the U.S. Air Force under Contract No. F19628-86-C-0138 with the Solid State Science Division, Rome Air Development Center, Hanscom Air Force Base.

*On leave from Institute of Molecular Physics, Polish Academy of Sciences, Poznań, Poland.

[1]G. Lehmann and W. J. Moore, J. Chem. Phys. **44**, 1741 (1966).
[2]G. Lehmann, Z. Naturforsch. **22a**, 2080 (1967).
[3]W. Becker and G. Lehmann, Solid State Commun. **35**, 367 (1980).
[4]J. Seifarth, U. Bartuch, and W. Karthe, Silikattechnik **32**, 276 (1981).
[5]M. J. Mombourquette, J. A. Weil, and W. C. Tennant, J. Chem. Phys. **85**, 68 (1986).
[6]J. A. Weil, T. Buch, and J. E. Clapp, Adv. Magn. Reson. **6**, 183 (1973).
[7]B. D. Perlson and J. A. Weil, Rev. Sci. Instrum. **46**, 874 (1975).
[8]R. H. D. Nuttall and J. A. Weil, Can. J. Phys. **59**, 1696 (1981).
[9]R. H. D. Nuttall and J. A. Weil, Solid State Commun. **33**, 99 (1980).
[10]J. A. Weil and J. H. Anderson, J. Chem. Phys. **35**, 1410 (1961).
[11]L. E. Halliburton, M. R. Hantehzadeh, J. Minge, M. J. Mombourquette, and J. A. Weil (unpublished).
[12]L. M. Matarrese, J. S. Wells, and R. L. Peterson, J. Chem. Phys. **50**, 2350 (1969).
[13]H. Rinneberg and J. A. Weil, J. Chem. Phys. **56**, 2019 (1972).
[14]M. J. Mombourquette and J. A. Weil, Can. J. Phys. **63**, 1282 (1985).